Journal 2006

+ Model

ARTICLE IN PRESS

ELSEVIER

Journal of Materials Processing Technology xxx (2005) xxx–xxx

Journal of Materials Processing Technology

www.elsevier.com/locate/jmatprotec

Microstructural evolution in the friction stir welded 6061 aluminum alloy (T6-temper condition) to copper

Jiahu Ouyang, Eswar Yarrapareddy, Radovan Kovacevic *

Research Center for Advanced Manufacturing, Department of Mechanical Engineering, Southern Methodist University, 1500 International Pkwy, Suite 100, Richardson, TX 75081, USA

Received 30 June 2004; received in revised form 19 April 2005; accepted 14 September 2005

Abstract

This paper concentrates on the temperature distribution and microstructural evolution of the friction stir welding of 6061 aluminum alloy (T6-temper condition) to copper. The mechanically mixed region in the joining of the dissimilar metals 6061 aluminum alloy and copper weld consists mainly of several intermetallic compounds such as $CuAl_2$, CuAl, and Cu_9Al_4 together with small amounts of α-Al and the saturated solid solution of Al in Cu. Distributed at the bottom of the weld nugget are numerous deformed copper lamellae with a high solid-solubility of aluminum. An intercalated structure or vertex flow pattern consisting of $CuAl_4$ and the saturated solid solution of Al in Cu is formed in the Cu-rich regions adjacent to the bottom of the weld by the mechanical integration of aluminum into copper. The measured peak temperature in the weld zone of the 6061 aluminum side reaches 580 °C, which is distinctly higher than the melting points of the Al–Cu eutectic or some of the hypo- and hyper-eutectic alloys. Higher peak temperatures are expected at the near interface regions between the weld metal and the stirred tool pin. The phases present in the welds can be explained from the Al–Cu equilibrium phase diagram with the assumption that a complete phase equilibrium is reached in the liquid state but not during solidification. The primary dendrites of α-Al, $CuAl_2$, and CuAl, and the eutectic of α-Al/$CuAl_2$ are formed in the weld nugget during solidification. Distinctly different micro-hardness levels from 136 to 760 $HV_{0.2}$ are produced corresponding to various microstructural features in the weld nugget.

Keywords: Friction stir welding; Joining of dissimilar metals; Intermetallic compounds

1. Introduction

Many emerging applications in power generation and the chemical, petrochemical, nuclear, aerospace, transportation, and electronics industries lead to the joining of dissimilar materials by different joining methods especially by friction welding and friction stir welding [1–8]. Due to the different chemical, mechanical, and thermal properties of materials, dissimilar materials joining presents more challenging problems than similar materials joining. However, when joining dissimilar materials by friction stir welding (FSW), the problems not only arise from a material properties point of view, but also from the possibility of the formation of brittle intermetallics and low melting point eutectics. The intermetallic compounds of Ti–Cu and Al–Cu systems were found in the friction welding of the copper–tungsten sintered alloy to pure titanium, the oxygen-free copper to pure aluminum [3,4], and in the cold roll welding of Al/Cu bimetal [5].

In the friction welding of the aluminum/steel system, intermetallic compounds are also a major problem [6]. From the joining process point of view, Al and Cu are incompatible metals because they have a high affinity to each other at temperatures higher than 120 °C and produce brittle, intermetallics on the interface [5]. Thus, solid-state welding processes such as explosion, friction, FSW, and cold roll welding have been considered as the qualified welding processes of these metals. Previous study [7] has introduced a relationship between the properties of joints and dissimilar materials that form brittle intermetallic compounds, and the time available for the formation of the compounds. It was claimed that satisfactory welds could be made if the welding conditions were such that the incubation period was longer than the welding time. However, the existence of incubation for the intermetallic formation is questionable and control should be based on limiting the thickness of the intermetallic compounds rather than on using an incubation period. Although problems exist due to high thermal conductivity, large

* Corresponding author. Tel.: +1 214 768 4865; fax: +1 214 768 0812.
E-mail address: kovacevi@engr.smu.edu (R. Kovacevic).

0924-0136/$ – see front matter © 2005 Elsevier B.V. All rights reserved.
doi:10.1016/j.jmatprotec.2005.09.013

differences in forging temperatures, and the formation of brittle intermetallic compounds, friction welding is probably acceptable within a limited range of the welding conditions [4–7]. In the friction welding of steel, it is questionable whether an asperity of melting occurs at the contact surface or not. However, an examination of the microstructures in the friction welded aluminum alloys and Al–SiC metal matrix composites, in peak-aged condition, indicate that a molten layer is present at the contact interface. This result has also been confirmed experimentally by in situ thermocouple measurements [8]. The lower melting temperature for such alloys is reported to be 555 °C. Localized melting of this kind has also been found during extrusion of the same materials at very high extrusion speeds [8].

The majority of previous studies [13–15] have primarily addressed the FSW of aluminum alloys to themselves in the thickness range of 1.6–12.7 mm. Of the aerospace alloys, the Al–Mg–Si, Al–Cu and Al–Zn series have been successfully friction stir welded with good tensile, bend, and fatigue properties. The FSW of a wide variety of both the same and dissimilar aluminum alloys to one another has been shown to involve dynamic recrystallization as the mechanism to accommodate the superplastic deformation that facilitates the bond [9–12]. Complex, fluid-like flow patterns often arise as a result of irregular lamellae formed by the flow of one recrystallized regime within or over another [1,9–12]. These features are also shown to characterize the FSW of 6061 aluminum to copper where equiaxed copper grains are observed to be roughly 1/5 the diameter of the 2–5 μm, equiaxed grains of 6061 aluminum alloy in the weld nugget [10]. However, it is quite difficult to achieve defect-free friction stir welds for a dissimilar 6061 aluminum alloy/copper system. There is usually a large void formation, cracks, and other distinct defects throughout the weld [1,9–12]. 6061 aluminum alloy and copper were friction stir welded with different tool rotations and welding speeds to achieve the void-free joint by shifting the tool insertion location with respect to the weld centerline [2]. The FSW of silver to AA 2024 aluminum alloy [10] demonstrated a rapid grain growth of silver when it was heavily deformed. The FSW of silver to AA2024 aluminum alloy represents an interesting joining method because the conventional fusion welding of silver to aluminum or aluminum alloys often produces brittle silver aluminide (Ag_3Al). In many applications, the formation of intermetallic phases completely comprises the integrity of the structure. A silver interlayer was also introduced to facilitate the conventional rotary friction welding of aluminum alloy to stainless steel where Ag_3Al was also formed but was not particularly deleterious [11].

In spite of extensive scientific interests in the FSW of dissimilar metals, no systematic study aiming to characterize the microstructural formation, material flow and interaction, and effects of temperature on microstructure and properties of dissimilar welds on thick metal plates appears to be available in the open literature. In this paper, a feasibility study of joining 6061 aluminum alloy to pure copper plates 12.7-mm thick by friction stir welding was performed. Different etching solutions were used to reveal and view the flow visualization and microstructural evolution throughout the FSW zone.

2. Experimental procedure

The experimental set-up consists of a vertical milling machine, two rotary acoustic emission (AE) sensors with amplifiers, a data acquisition system based on a PC, an infrared camera with an image capturing board, a specially designed tool, rigid fixing, and samples for butt welding, as shown in Fig. 1a. All the welds were made in a butt-weld configuration. Fig. 1b shows the configuration of 6061 aluminum alloy and copper plates for dissimilar metal welds. The material used for the tool shoulder is typical tool steel. The tool pin material is a tool steel grade with a good balance of abrasive resistance, strength, and fracture toughness. The diameter of the stirring pin is about 12 mm. The 6061-T6 aluminum rolled plate is 12.7 mm in thickness with a chemical composition of (wt%) 0.7 Si, 0.7 Fe, 0.1 Mn, 1.0 Mg, 0.4 Cu, 0.1 Cr, 0.25 Zn, 0.15 Ti, and balance Al. The copper is 99.99 wt% rolled plate with the same thickness. The 6061 aluminum alloy rolled plates are solution heat treated at about 520 °C and artificially aged at about 160 °C for about 18 h. A number of FSW experiments of 6061 aluminum alloy to copper were carried out to obtain the optimum parameters by adjusting the rotational speed of the tool and the welding speed in the range of 151–1400 rpm and 57–330 mm/min, respectively. Other parameters including the threaded geometry and plunge depth of the stir pin were kept constant.

Temperatures in the weld zone were measured by K-type thermocouples imbedded at different positions (8.0–25 mm) from the joint line through a series of small holes (2.5 mm in diameter) drilled from the side of the 6061 aluminum alloy plate as shown in Fig. 1c. These holes were located at the mid-regions of the length direction to allow the steady weld to be developed. The preliminary experiments demonstrate that the recorded temperature difference from the start to the end of the weld was about 30 °C due to the build-up of heat input for the weld of 180.00 mm in length and 12.7 mm in thickness. It was assumed that the presence of these drilled holes would not have an affect on the temperature filed. Two sets (2.0 and 8.0 mm deep from the weld surface) of the holes as shown in Fig. 1c were used to measure the temperature variations at different positions along the thickness. The thermocouple were inserted and then sealed to the bottom of the holes from the 6061 aluminum alloy side. The values of temperature were recorded at 2 Hz digitally using the corresponding data acquisition system.

For microstructural analysis, the welds were sectioned longitudinally and cross-sectionally as shown in Fig. 1b. The cross sectional direction locations of the samples taken for the microstructural analysis were shown in Fig. 2. The sectioned samples were prepared using standard metallographic procedures. The samples were etched using a modified Keller's reagent (nominally; 150 ml water, 3 ml nitric acid, 6 ml hydrochloric acid, and 6 ml hydrofluoric) for the 6061 aluminum alloy side. The copper side was etched with a solution consisting of 100 ml of water, 4 ml of saturated sodium chloride, 2 g of potassium dichromate, and 5 ml of sulfuric acid. Observations of plastic deformation, material flow, and microstructure were performed using a high-resolution optical microscope and an electron probe. Vickers microhardness measurements were performed on both the cross- and longitudinal sections of the welds using a microhardness tester at a 200-g load and a 15-s dwell time. Three different longitudinal sections at the weld centerline, and the welded regions both in the 6061 aluminum alloy and copper sides both at 4 mm from the weld centerline, respectively, were prepared for the X-ray diffraction (XRD) phase analysis. The phase structures of dissimilar 6061 aluminum alloy/copper welds were studied using the XRD system with 40-Kv operating voltage and Cu Kα radiation. A scanning program with a step scanning rate of 0.04° mm^{-1} was employed to determine the peak positions of different phases in the range of $10° < 2\theta < 100°$. A standard procedure called energy dispersive spectroscopy (EDS) was used for identifying and quantifying the elemental compositions of phases formed during the FSW of 6061 aluminum alloy and copper.

3. Results and discussion

3.1. Weld temperature history

The relationship between the temperature profile variations and time under the welding conditions of the rotational speed of 914 rpm and a welding speed of 95 mm/min is shown in Fig. 3. The maximum temperature reached at the position I of 8 mm

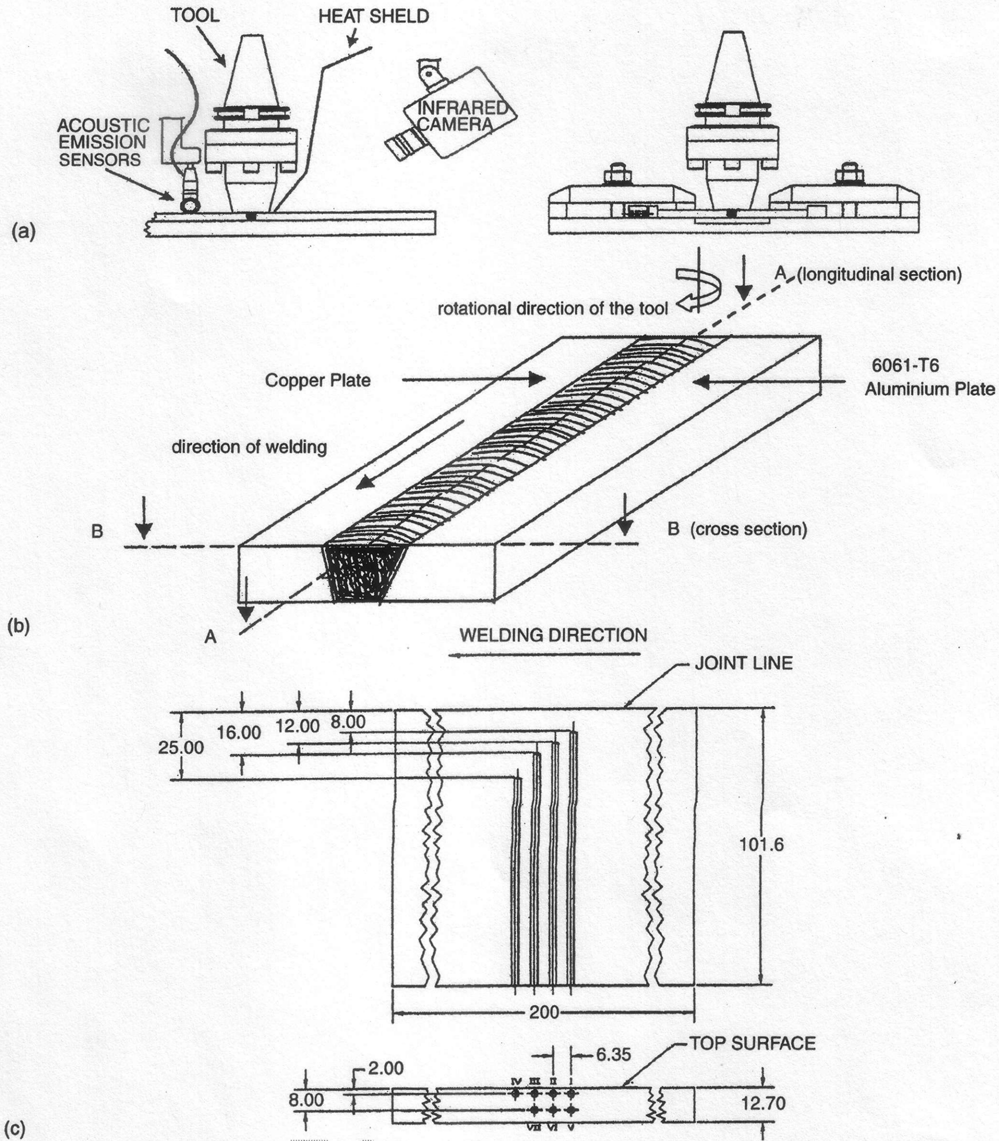

Fig. 1. Experimental set-up and weld configuration: (a) experimental set-up; (b) schematic diagram showing the positions of the samples taken from different sections of the welds; (c) schematic diagram showing the positions of thermocouples imbedded into the 6061 aluminum alloy plate.

from the joint line is about 580 °C, which is slightly lower than the solidus-line melting point (582 °C) of the 6061 aluminum alloy. The holding time of the welded material at above 500 °C is extremely short ($t = 24$ s). There is a decrease trend in the

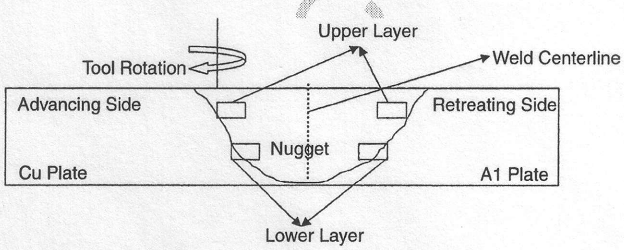

Fig. 2. The cross sectional view representation of friction stir welded 6061 aluminum alloy and copper plate showing the positions upper layer, lower layer and the weld nugget.

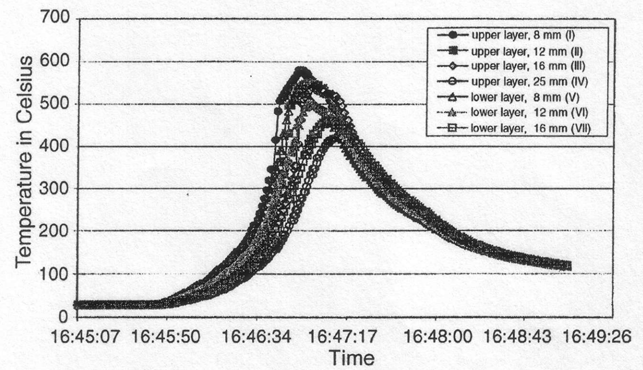

Fig. 3. Relationship between the measured temperature profile variations in the weld zone and the time under the welding condition of 914 rpm for rotational speed and 95 mm/min for welding speed. Curves represent the temperature history at different positions (positions I–VII as shown in Fig. 1c from the weld centerline or from the top surface.

peak temperature with changing the measurement positions from 8 mm (position I) to 25 mm (position IV) from the joint line. The peak temperature at the position IV, which is close to the edge of the shoulder, is about 420 °C. From the temperature data shown in Fig. 3, the peak temperature at different depths of 2 mm (positions I–IV) to 8 m (positions V–VII) from the top surface are also distinctly different. The thermocouples (positions I–III) at the upper layer recorded higher values of temperature than those (positions V–VII) at the lower layer. The quality of the joints is judged from the weld appearance and whether there are internal defects or not. Metallographic examinations of the welds show that the thermocouples near the tool pin are not destroyed by the stirring action but do change positions slightly due to the mechanical mixing. Although the measured peak temperatures at the 6061 aluminum alloy side are lower than the melting points of both the 6061 aluminum alloy and copper, the peak temperature is clearly higher than the melting points of Al–Cu eutectic or some of the hyper-eutectic alloys. Higher peak temperatures are expected more inside the weld nugget than outside the nugget. It is assumed that the temperature profile at the 6061 aluminum alloy side to be symmetrical with respect to the 6061 aluminum alloy/copper system. Elevated temperatures in the weld reduce the metal flow stress and the torque that limits any power generation increase. The yield strength of the 6061 aluminum alloy at 371 °C is 15 MPa, which is much lower than that yield strength at room temperature (280 MPa) [13]. While the temperatures in the weld zone remain high for a short time, dynamic recrystallization and localized melting may occur to provide an instantaneous two-phase flow due to the stirring action. A distinct melting phenomenon is also verified by the microstructural features in the weld nugget as mentioned in Section 3.3.

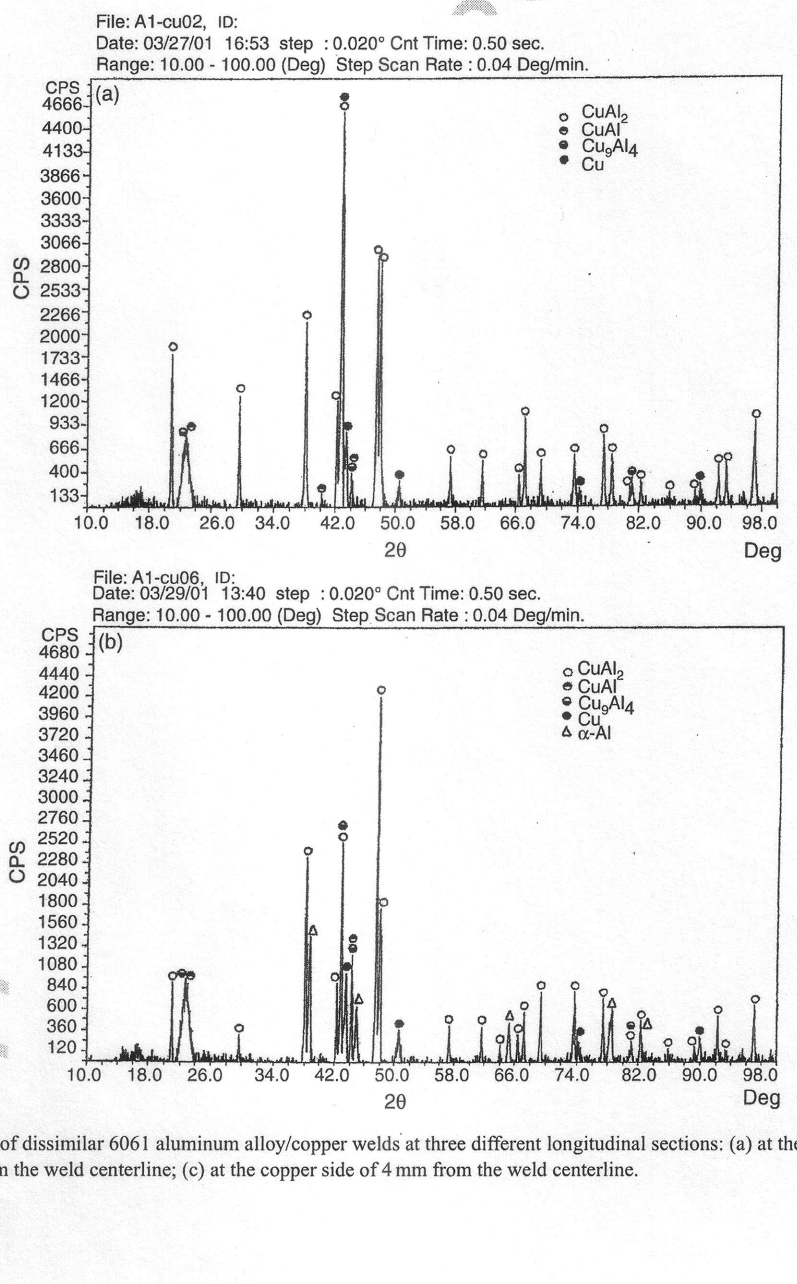

Fig. 4. X-ray diffraction patterns of dissimilar 6061 aluminum alloy/copper welds at three different longitudinal sections: (a) at the weld centerline; (b) at the 6061 aluminum alloy side of 4 mm from the weld centerline; (c) at the copper side of 4 mm from the weld centerline.

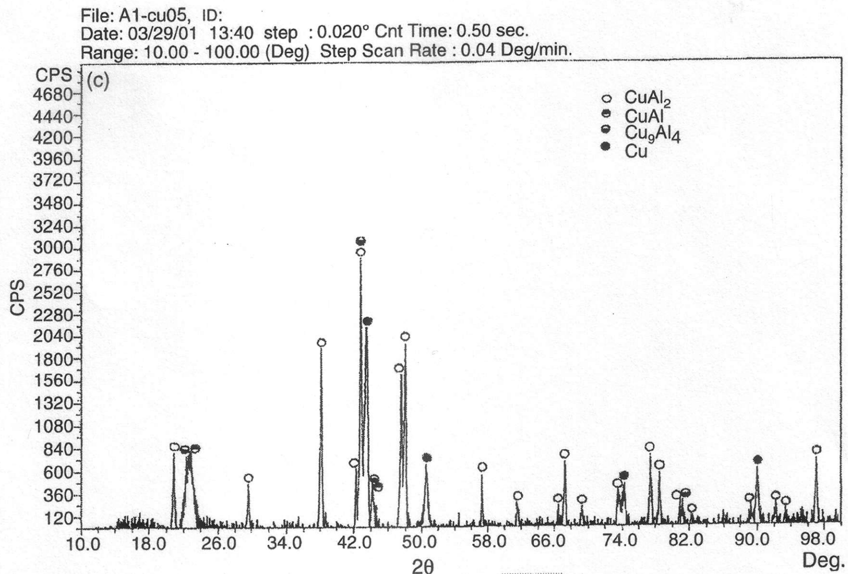

Fig. 4. (*Continued*).

3.2. Phase analysis of the dissimilar 6061 aluminum alloy/copper welds

Fig. 4 shows X-ray diffraction patterns of dissimilar 6061 aluminum alloy/copper welds at three different cross sectional locations: the weld centerline, and the 6061 aluminum alloy and copper sides both at 4 mm from the weld centerline. The results illustrate that the weld of 6061 aluminum alloy to copper consists mainly of the intermetallic compounds such as $CuAl_2$, CuAl, and Cu_9Al_4 together with some amounts of α-Al and Cu (saturated solid solution of Al in copper). More of the single phases of α-Al and copper are detected near the 6061 aluminum alloy side as well as the dominant intermetallic compounds as shown in Fig. 4b. However, as shown in Fig. 4c, no distinct α-Al peak is found, and more of the single phase of copper is detected near the copper side as shown in Fig. 4a. The variations of copper, α-Al, and intermetallic compound peaks corroborate the complex mixing of copper and 6061 aluminum alloy grains in the weld zone. According to the X-ray diffraction results, the high temperatures associated with the strong stirring action tool pin cause the heterogeneous mixing of Al and Cu and results in the formation of intermetallic compounds $CuAl_2$, CuAl, and Cu_9Al_4. Stronger $CuAl_2$ peaks than those of CuAl and Cu_9Al_4 in the weld zone indicate an insufficient interaction time in spite of the strong stirring action of the tool pin. From Fig. 4, the peaks of the face centered cubic Cu, Cu_9Al_4, and CuAl phases are clearly widened because of the excessive solid solution of aluminum into these phases [16]. From the Al–Cu phase diagram [17], the face-centered cubic copper, Cu_9Al_4, and CuAl crystals generally exhibit wide phase fields accompanied by the changes of aluminum concentration in the copper. A face-centered cubic copper structure with a wide composition range of aluminum is mainly distributed at the bottom of the weld nugget. The ratio of aluminum over copper content is found to vary by as much as 15.5 at. wt% in the single Cu phase. Similar results are also found by Aritoshi et al. [3] in the friction welding of the copper-tungsten sintered alloy to pure titanium, and the oxygen-free copper to pure aluminum.

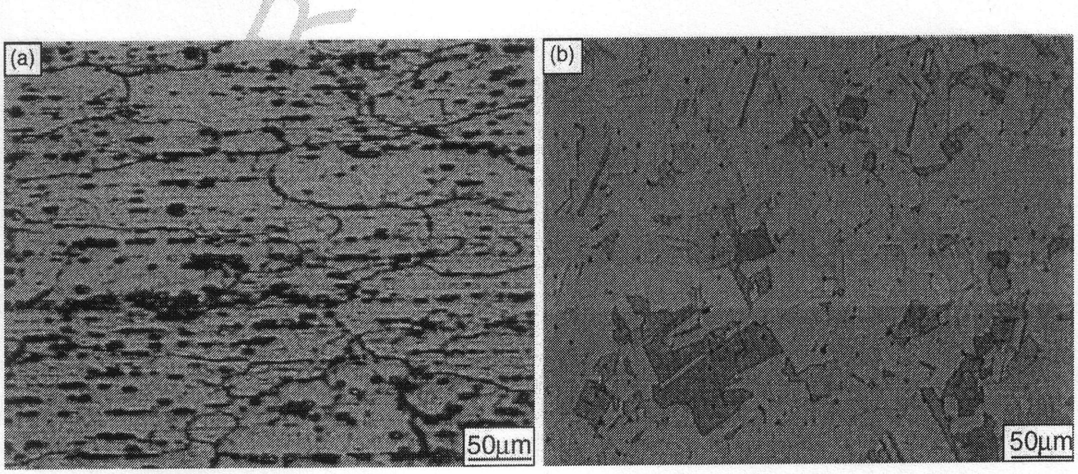

Fig. 5. Microstructures of the substrates of (a) 6061 aluminum alloy (T6 temper condition) and (b) copper.

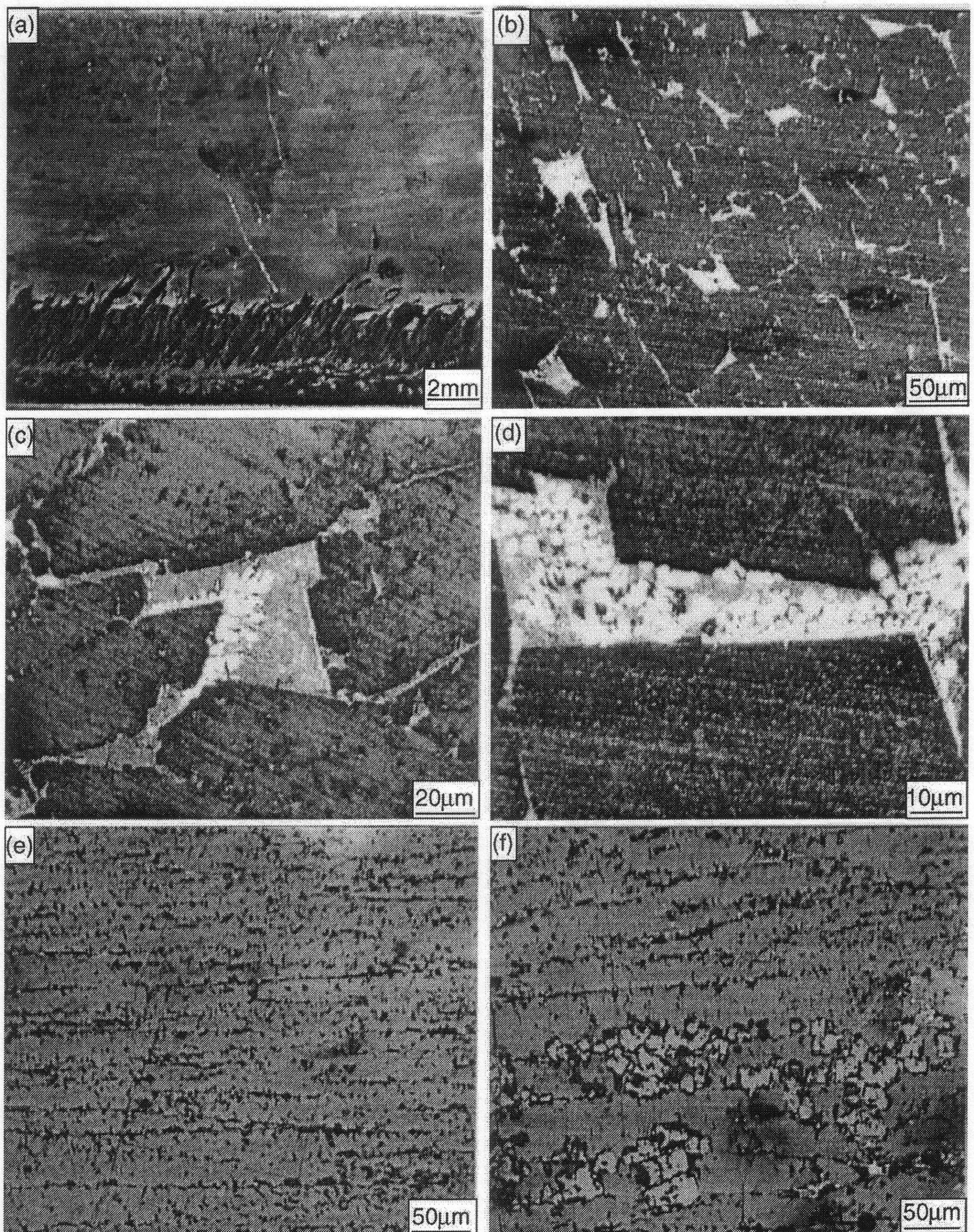

Fig. 6. A through thickness longitudinal direction of a dissimilar 6061 aluminum alloy/copper weld at a rotational speed of 914 rpm and a welding speed of 95 mm/min: (a) morphology at low magnification; (b) microstructure at the upper layer; (c) and (d) α-Al primary dendrite and eutectic of α-Al/$CuAl_2$ at the upper layer; (e) orientated growth of $CuAl_2$ crystals at intermediate layer; (f) localized defect wall structure of $CuAl_2$.

3.3. Weld microstructure of dissimilar 6061 aluminum alloy/copper welds

The microstructures of the parent materials 6061 aluminum alloy and copper are shown in Fig. 5. The grains of the 6061 aluminum alloy are elongated along the rolled direction as shown in Fig. 5a. The copper substrate exhibits an irregular grain shape and a wide size range of 10–50 μm as shown in Fig. 5b. A through-thickness longitudinal section of the dissimilar 6061 aluminum alloy/copper weld at a rotational speed of 914 rpm and a welding speed of 95 mm/min is shown in Fig. 6. In addition to the macrocracks that are always present as shown in Fig. 6a, regardless of the welding parameters used, etching reveals that the weld contains some microcracks and solidified defects as shown in Fig. 6e. From Figs. 6b–d, it can be seen that the upper layer of the weld nugget consists of mainly

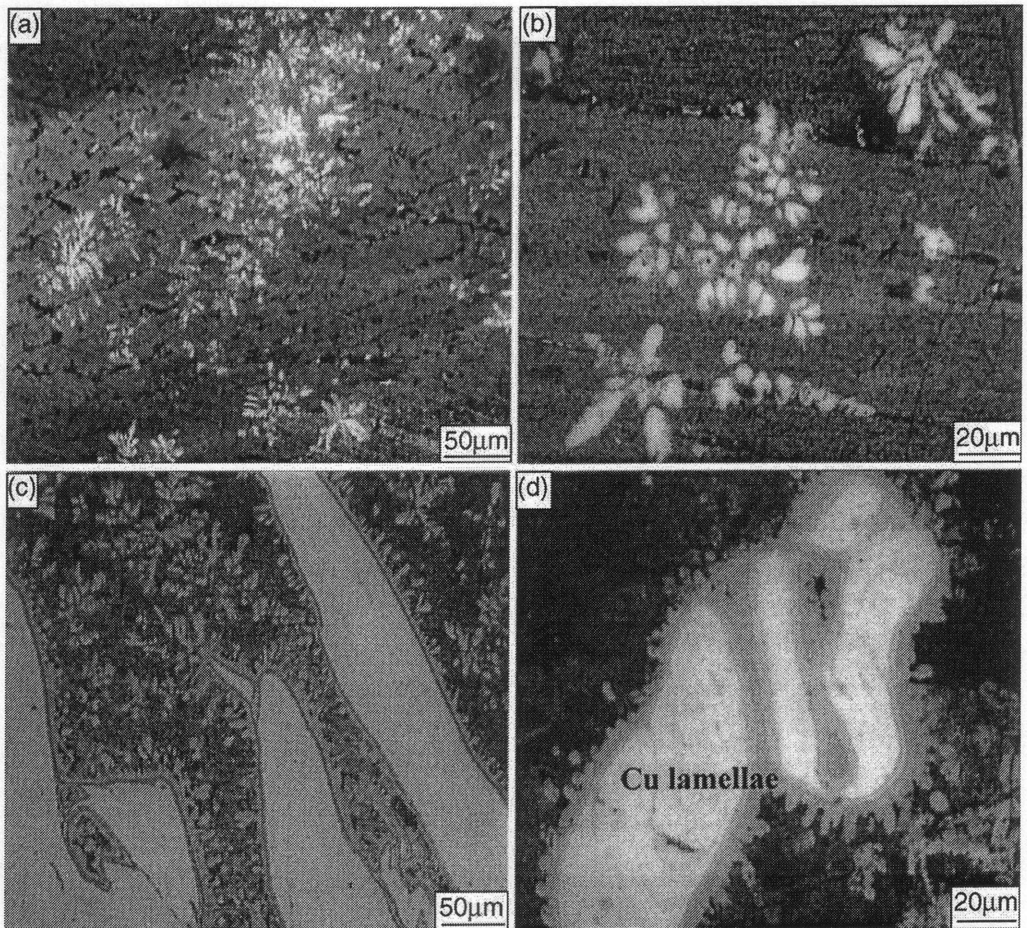

Fig. 7. The morphology of CuAl intermetallic compound: (a) CuAl primary dendrites independently nucleated from the liquid phase; (b) enlarged views of CuAl dendrites; (c) and (d) CuAl precipitation at the edges of the deformed Cu lamellae.

of $CuAl_2$ grains, and α-Al primary dendrites and eutectics of α-Al/$CuAl_2$ at the grain boundary regions. The $CuAl_2$ grains have a size range of 30–80 μm at the upper layer. The α-Al primary dendrites exhibit a flower-like or particle shape where the size of the α-Al/$CuAl_2$ eutectic is typically less than 1 μm. However, in the intermediate layer, the $CuAl_2$ crystals exhibit clearly the characteristic of oriented growth. No α-Al primary dendrite or α-Al/$CuAl_2$ eutectic is found at the grain boundary regions. The average chemical composition measured from energy dispersive spectroscopy (EDS) results is (at. wt%) 32.4 Cu and 67.6 Al at the interior of grains. Metallurgical observations show that the orientation of the $CuAl_2$ crystals in the intermediate layer is nearly constant over very long distances (400 μm) as shown in Fig. 6e. Small orientation changes are observed over distances less than 10 μm. A part of the orientation changes is localized in the defective structure and part is due to the cumulative effect of faults as shown in Fig. 6f. Macrocracks could be observed running through the $CuAl_2$ grains (Fig. 6e).

The morphologies of the CuAl intermetallic compound are shown in Fig. 7. The flower-like primary dendrites are clearly observed at the lower layer of the weld nugget as shown in Fig. 7a and b. The EDS data show that the chemical composition of these dendrites is (at. wt%) 49.2 Cu and 50.8 Al. These CuAl primary dendrites typically have a size less than 10 μm. These dendrites are believed to independently nucleate and grow directly from the liquid phase as shown in Fig. 7a–d and show the morphology of the radiated and cylindrically growth of the CuAl crystals at the edges of the deformed copper lamellae. The EDS analysis indicates that the concentration of copper in these CuAl crystals at the edge of the copper lamellae is about 54.3 at. wt%, which is slightly higher than that of the independently nucleated CuAl dendrites. Flower-like CuAl dendrites are typically observed at the lower regions that are close to copper lamellae. Only the primary arms of the dendrites are fully developed. From Fig. 7a and b, it can be also seen that the $CuAl_2$ crystals exhibit an oriented growth and a larger size than CuAl dendrites. The intermetallic compounds of $CuAl_2$ and CuAl in an Al–Cu alloy system were also detected with different morphologies at the narrow weld zone in both the friction welding of oxygen-free copper to pure aluminum [3] and the cold roll welding of Al/Cu bimetal.

Fig. 8 shows the enlarged views of alternative Cu/Cu_9Al_4 lamellae or vortices that appear near the bottom of the weld nugget. The bright regions are unmixed Cu lamellae with a hardness range of 78–85 $HV_{0.2}$, while the dark Cu-rich regions are

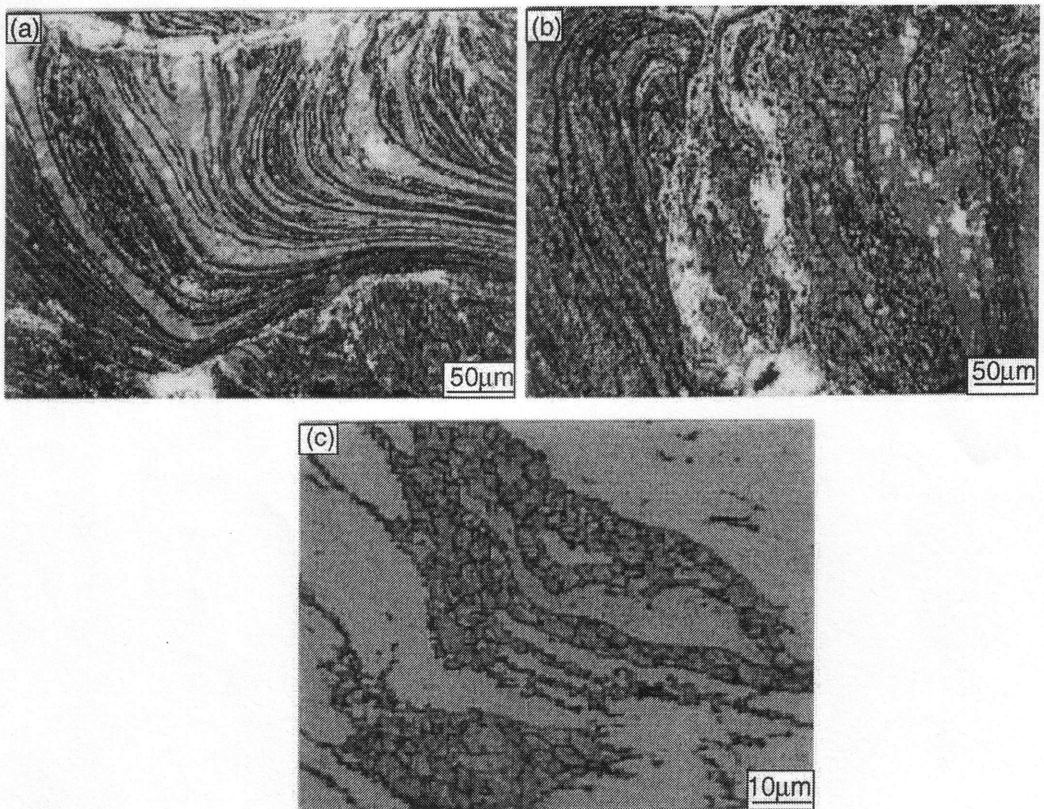

Fig. 8. Enlarged views of alternative Cu/Cu_9Al_4 lamellae or vortices: (a) material flow pattern at the bottom of the weld nugget; (b) alternative lamellae near the copper side of the weld; (c) some details of Cu_9Al_4.

mixed with some amounts of aluminum by the strong stirring action of the tool pin. The intercalated regions appear to be an overlapping saturated solid solution of Al in Cu and Cu_9Al_4. The concentration of copper at the dark Cu-rich regions is in the range of 66.2–94.6 at. wt%. These dark Cu-rich regions with a hardness range of 136–178 $HV_{0.2}$ are considered to contain a certain percentage of the Cu_9Al_4 intermetallic compound. The interface of solid state welded Al/Cu is susceptible to the nucleation and growth of intermetallic compounds at temperatures greater than 120 °C [5]. This process is thermally activated. By increasing the temperature, the nucleation and growth of the compounds are accelerated. A distinct difference in color from red to yellow is also observed in the deformed copper lamellae at the bottom of the weld nugget using optical microscopy. Fig. 8b shows the alternative lamellae near the copper side of the weld. The dark regions as shown in Fig. 8c illustrate some details of Cu_9Al_4 lamellae, which have a composition of (at. wt%) 32.5 Al, 67.2 Cu, 0.2 Mg and 0.1 Si. No 6061 aluminum alloy lamella is found in the observed material flow patterns. This result is much different from the results by Murr et al. [9–11]. However, there is great a solubility of aluminum in copper. The phase filed of single FCC Cu phase is very wide with a composition range of aluminum up to 20 at. wt% in the Al–Cu binary phase diagram as shown in Fig. 9. Almost all of aluminum stirred to Cu at the Cu-rich side of the weld nugget is found to form a saturated solid solution of Al in a Cu or Cu_9Al_4 intermetallic compound under these experimental conditions. A perusal of the intercalated vortex, swirl-like, and more complex solid-state shear structures for the mechanical integration of aluminum into copper enables not only the visualization of fascinating solid-state flow phenomena, but also complex interdiffusion and interaction of the two materials.

The microstructural features of cross-sections of a dissimilar 6061 aluminum alloy/copper weld obtained under the condition of 914 rpm for rotational speed and 95 mm/min for welding speed are shown in Fig. 10. One of the particularly interesting features is the microstructural change at the transition zones.

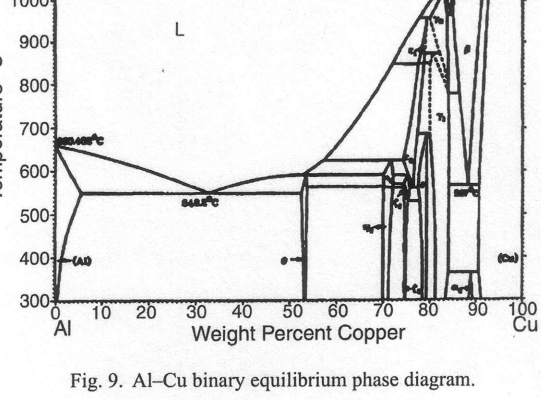

Fig. 9. Al–Cu binary equilibrium phase diagram.

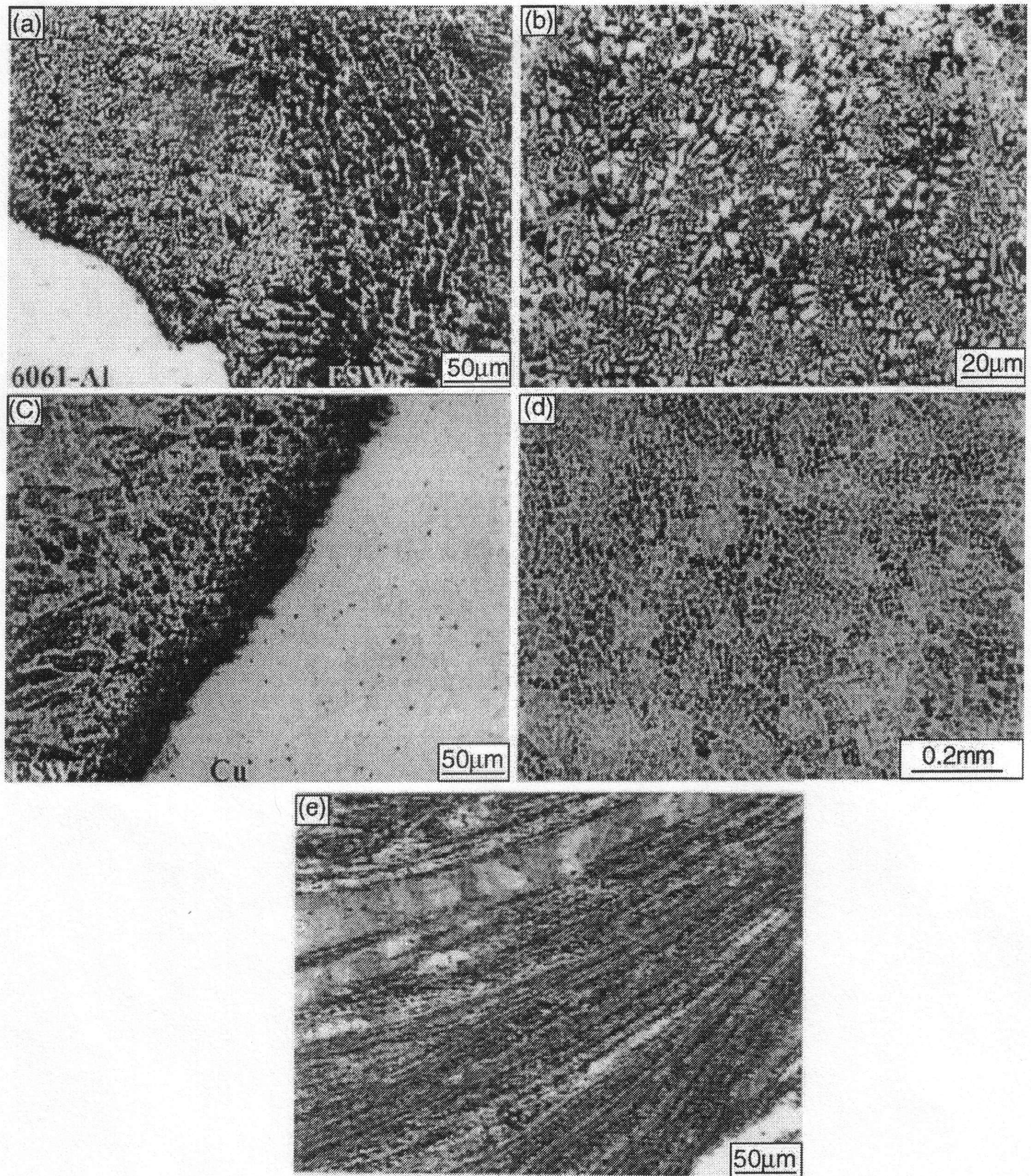

Fig. 10. Microstructural features of cross-sections of a dissimilar 6061 aluminum alloy/copper weld under the condition of 914 rpm for rotational speed and 95 mm/min for welding speed: (a) 6061 aluminum alloy/FSW transition zone; (b) enlarged morphology of α-Al/$CuCl_2$ eutectic; (c) FSW/copper transition zone; (d) morphology of intermetallic compound at the center of weld cross-section; (e) material flow patterns at the bottom of the weld cross-section.

From the 6061 aluminum alloy side to the FSW zone, the mechanical integration of copper into aluminum causes the formation of an α-Al/$CuAl_2$ eutectic and $CuAl_2$ intermetallic compound grains as shown in Fig. 10a. The thickness of the transition zone featured by the α-Al/$CuAl_2$ eutectic is about 100 µm. Fig. 10b shows the enlarged morphology of an α-Al/$CuAl_2$ eutectic. The presence of a eutectic phase in the structure of the transition zone is confirmed by the results of XRD data and microstructural observations. Some coarse α-Al grains are also observed near the transition zone as shown in Fig. 10b. The EDS microanalysis establishes that in this zone a hypoeutectic alloy with a composition (at. wt%) of 13.3 Cu, 86.1 Al, 0.4 Mg, and 0.2 Si forms. The microstructural feature of the FSW/copper transition zone is shown in Fig. 10c. The relatively coarse $CuAl_2$ grains are clearly observed at the transition zone of the copper side. Fig. 10d shows the morphology of the intermetallic compound at the center of the weld cross-section. Fine $CuAl_2$ grains are observed from the weld cross section. It is concluded that the stirring action causes the formation of a weld cross section to develop a low melting point hypoeutectic or eutectic Al–Cu alloys at the 6061 aluminum alloy/FSW side, and a hypereutectic alloy at the center of the weld nugget and FSW zone/copper side. The material flow patterns at the bottom of the weld-cross section are shown in Fig. 10e. A solid solution of aluminum

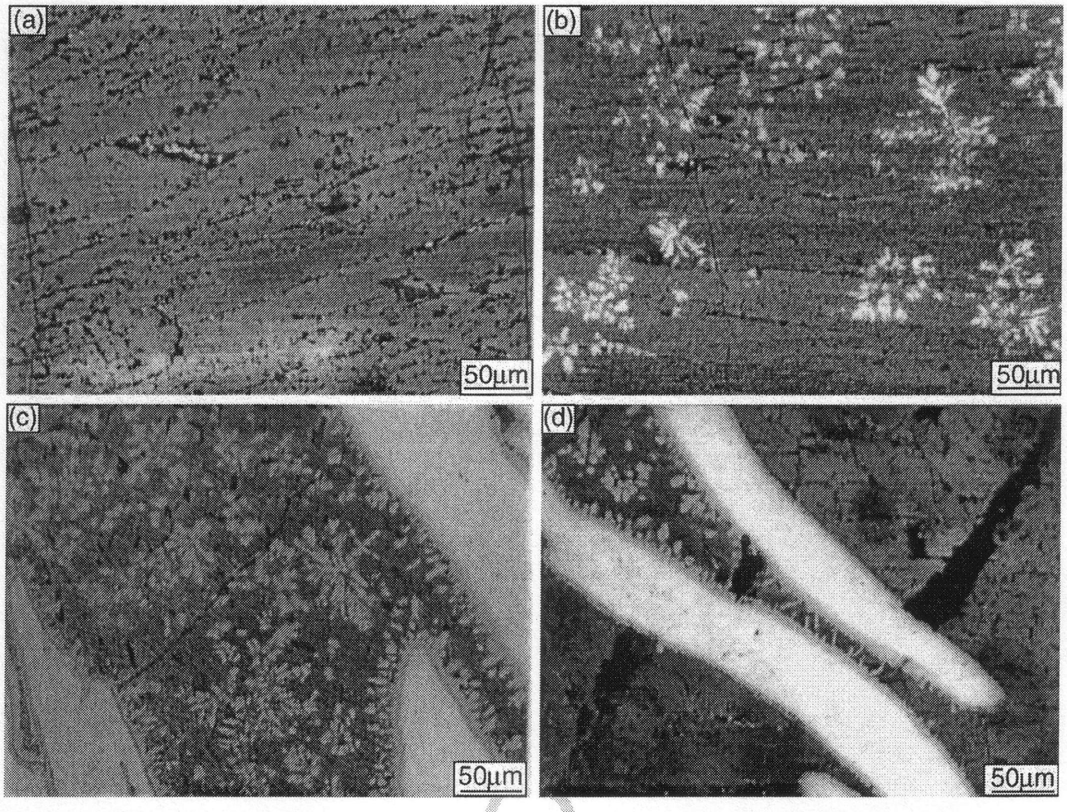

Fig. 11. Morphology of the cracks formed in different microstructural regions of the weld nugget: (a) in the intermediate layer; (b) at the lower layer; (c) at the bottom of the weld nugget; (d) crack bridge-connection between the deformed copper lamellae.

in copper predominates at the bottom, and no liquid phase is developed by the stirring action and thermal activation by friction forces.

The majority of the 6061 aluminum alloy/copper welds exhibits a considerable discontinuity and crack propagation, and they are not good welds. Some welds fail due to the thermal cracking and lack of bonding. Nonetheless, continuous regions could be used to examine the microstructure and the corresponding hardness profiles. Fig. 11 shows the morphology of cracks formed in different microstructural regions of the weld nugget. The cracks are often observed to run perpendicular to the growth direction of $CuAl_2$ crystals as shown in Fig. 11a and b. Almost no distinct crack networks are found in the weld zone. The cracks may first originate within the interior of the $CuAl_2$ grains, where local elastic thermal stress concentration may be beyond the fracture strength of $CuAl_2$ A lot of cracks may occur due to some accumulation of alloying elements as a result of a temperature rise and the existence of intermetallic layers such as $CuAl_2$. There exists no distinct effect of CuAl primary dendrites on the crack propagation. It is noted that more cracks are found in the intermetallic layer of $CuAl_2$ of the mid-radius of the weld than at both the sides and periphery of the weld. Some cracks initiate and then propagate through the $CuAl_2$ grains between the deformed copper lamellae as shown in Fig. 11c and d. In this case, the ductile copper lamellae are beneficial to restrain or deflect the microcracks by a bridge-connection mechanism as shown in Fig. 11d.

The microhardness measurements of a through-thickness 6061 aluminum alloy/copper weld under the welding condition of 914 rpm for the rotational speed and 95 mm/min for the welding speed are performed using a Vickers microhardness tester. The hardness of the unaffected parent metal is in the range of 90–100 $HV_{0.2}$ for the 6061 aluminum alloy and 75–85 $HV_{0.2}$ for the copper, respectively. The minimum value is about 65 $HV_{0.2}$ in the heat-affected zone (HAZ) of the 6061 aluminum alloy. Fig. 12 shows significant variations in hardness at different microstructural regions of the weld zone. There is a fluctuating hardness (136–760 $HV_{0.2}$) in the weld nugget that is related to different microstructures of intermetallic compounds and material flow patterns. The hardness and tensile strength of the intermetallic compounds are distinctly higher than those of both the 6061 aluminum alloy and the copper. The hardness of $CuAl_2$ grains at the upper layer or intermediate layer is measured to be 486–557 $HV_{0.2}$, while the hardness of the α-Al/$CuAl_2$ eutectic is about 257–385 $HV_{0.2}$ at the grain boundary regions as shown in Fig. 12b and c. The hardness of the CuAl primary dendrites at the lower layer is about 663–760 $HV_{0.2}$, while the hardness of the intercalated lamellae of Cu_9Al_4/saturated solid solution of Al in Cu is about 136–178 $HV_{0.2}$, higher than that of the copper substrate as shown in Fig. 12a, c and d. As can be seen by comparing the microstructure and measured thickness, there is a good correlation between the hardness and distribution of different phases caused by the material flow and interaction. Microhardness variations are common throughout the weld

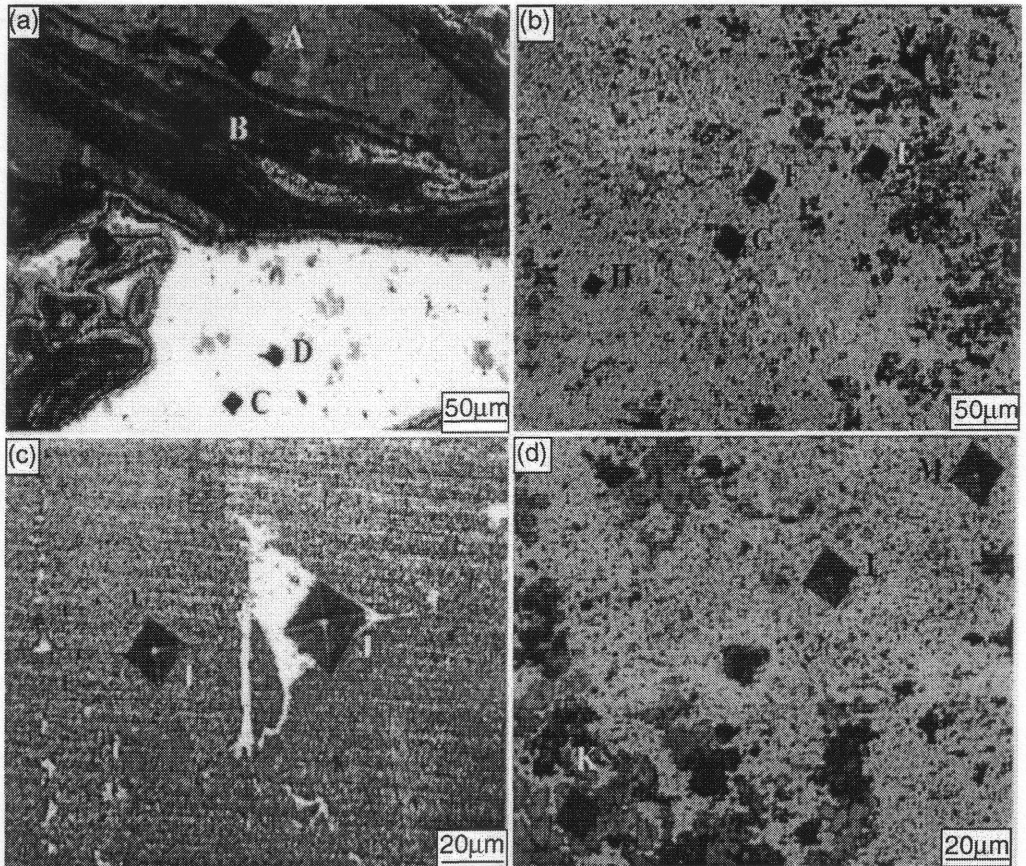

Fig. 12. The indents showing significant variations in microhardness at different microstructural regions (marked by characters A–M) of the weld zone under the welding condition of 914 rpm for rotational speed and 95 mm/min for welding speed: (a) indents on intercalated lamellae (marked by A and B) and $CuCl_2$ grains (marked by C and D); (b) indents on CuAl dendrite (marked by E), α-Al/$CuAl_2$ eutectic (marked by F and G) and $CuAl_2$ grains (marked by H); (c) enlarged indents on $CuAl_2$ grain (marked by I) and eutectic of α-Al/$CuAl_2$ (marked by J); (d) enlarged indents on CuAl dendrite (marked by K) and $CuAl_2$ (marked by L and M).

zone as a consequence of the variations in microstructures such as intermetallic compounds, grain size, density, thickness, and intercalation periodicity.

3.4. Discussion

The FSW of 6061 aluminum alloy to copper is not only notably influenced by the welding parameters, but a more contiguous weld occurred at 914 rpm for the rotational speed and 95 mm/min for the welding speed. One of the reasons for attempting to weld copper and 6061 aluminum alloy in this study is to examine the material interaction and flow phenomena in more detail by observing the mixing of the copper and 6061 aluminum alloy. Complex microstructural issues are found in a 6061 aluminum alloy/copper system where intermetallic compounds can form as a consequence of temperature variations (well below the melting point of the parent metals) and a wide range of compositional fluctuations. Some of these features are discussed below in detail for the formation of intermetallic compounds and subsequent solidification.

In a dissimilar 6061 aluminum alloy/copper weld, a mixed layer of aluminum and copper that includes brittle intermetallic compounds such as $CuCl_2$, CuAl, and Cu_9Al_4 are formed from the XRD results and microstructural observations. It is considered that the softening of the stirred 6061 aluminum alloy facilitates the formation of the mixed layer and intermetallic compounds. Unlike a friction stir welding process, a mixed layer containing a large amount of intermetallic compounds is hardly excluded by the forging forces and in situ extrusion action during FSW. It is well known that the thickness of a mixed intermetallic compound layer may be controlled by the adjustment of the forge pressure and rotational speed in the friction welding [3,4]. A consensus has not been reached upon the mechanism of the phase transformation when small amounts of Cu is stirred into the 6061 aluminum alloy at elevated temperatures during FSW. One great source of difficulty is the low solubility of copper in aluminum, and the existence of different intermetallic phases under the welding conditions. Almost all of the copper stirred into the 6061 aluminum alloy is found to form the intermetallic compounds under these experimental conditions. However, the situation is different when aluminum is stirred into the copper. A saturated solid solution is formed because of the great solubility of aluminum in copper.

The formation of intermetallic compounds can be understood by an analysis of the Al–Cu binary phase diagram as shown in Fig. 9. However, it should be kept in mind that the figure represents an equilibrium phase diagram and is, therefore, inadequate to represent some of the rapid thermal changes taking place during FSW. It is assumed that the reaction time is long enough for liquid state reactions to reach equilibrium, and good mixing in the weld is obtained by the strong stirring action of the tool pin. The liquidus line of the Al–Cu phase diagram as shown in Fig. 9 indicates a peritectic reaction $L+\varepsilon_1 \rightarrow \eta_1$ at about 620 °C and a peritectic reaction $L+\eta_1 \rightarrow \theta$ at 590 °C in the liquid state resulting in the formation of the η_1 (CuAl) and θ ($CuAl_2$) phase directly from the liquid phase, and a eutectic reaction $L \rightarrow \alpha\text{-Al}+\theta$ at 548.3 °C resulting in the formation of the α-Al/$CuAl_2$ eutectic products. Although the measured peak temperature at position I is 580 °C, much higher temperatures are expected at the near-interface regions between the weld metal and the tool pin. The $CuAl_2$ phase predominates at the longitudinal section of the weld centerline due to its low melting point and the strong action described above during FSW.

A complex intercalated structure or vortices of Cu_9Al_4 and the saturated solid solution of Al in Cu are formed at the bottom of the weld nugget or Cu-rich regions by mechanical integration of the aluminum into copper. The formation of Cu_9Al_4 intermetallic compound having a fine grain structure is probably due to the mechanical mixing and interaction in the solid state. The peak temperatures measured with the thermocouples imbedded near the pin tool are much lower than the melting points of copper-rich alloys located at the right side of the Al–Cu phase diagram; although, it is higher than the eutectic temperature of the Al–Cu system. The formation reasons of Cu_9Al_4 are probably attributed to the following: (1) the mechanical mixing due to the stirring action of the pin tool that produces some localized regions with a similar compositional range to Cu_9Al_4; (2) the dissolution at the friction surface; and (3) the interdiffusion along the grain boundaries. The interface of solid state welded Al/Cu is susceptible to the nucleation and growth intermetallic compounds at temperatures greater than 120 °C [5]. Similar results of the Cu_9Al_4 phase were also reported in the friction welding of oxygen-free copper to pure aluminum by Aritoshi [3]. As the melting point of the α-Al/$CuAl_2$ eutectic is as low as 548.3 °C, it is possible for the weld metals with suitable compositions in the Al–Cu system to be melted during the FSW. The interdiffusion rates of aluminum and copper atoms in the liquid phase are much larger than those in the solid solution. In this case, the growth rate of the intermetallic compound layers is very rapid. The melting of the weld metals reduces the viscosity coefficient of the weld zone and makes the stirring action of the pin tool become a relatively easy process. The softened layer has also been considered as a viscous fluid with a large viscosity. Another intriguing issue associated with a dissimilar 6061 aluminum alloy/copper weld is the intercalated microstructure of Cu_9Al_4 and the deformed Cu solid solution. The metallographic examinations prove difficult due to the formation of a polishing step at the interface. This formation makes an accurate measurement of the thickness of the Cu_9Al_4 intermetallic layer very difficult. The thickness of Cu_9Al_4 is mainly dependent upon the heat input and mass input of aluminum into the weld. These features also produce distinct hardness fluctuations and further affect the properties of the welded metals.

4. Conclusions

From the performed analysis, the following conclusions can be derived:

(1) Direct FSW of 6061 aluminum alloy to copper has proved difficult due to the brittle nature of the intermetallic compounds formed in the weld nugget. It is suggested to use a kind of interlayer to produce sound welds.
(2) The mechanically mixed region in a dissimilar 6061 aluminum alloy/copper weld consists mainly of several intermetallic compounds such as $CuAl_2$, CuAl, and Cu_9Al_4 together with small amounts of α-Al and a face-centered cubic solid solution of Al in Cu. Distributed at the bottom of the weld nugget are the deformed copper lamellae with a solid solubility of aluminum. A mixed layer of Cu_9Al_4 and the deformed Cu solid solution that showed an intercalated microstructure or vortex flow pattern is formed in copper adjacent to the bottom of the weld by the mechanical integration of aluminum into copper. Distinctly different microhardness levels from 136 to 760 $HV_{0.2}$ were produced in the weld nugget corresponding to various microstructures and material flow patterns.
(3) The peak temperature measured in the weld zone of the 6061 aluminum alloy side is up to 580 °C, distinctly higher than the melting points of an Al–Cu eutectic or some of hypo- and hyper-eutectic alloys. A higher peak temperature is expected at the interface regions between the weld metal and tool pin. The phases present in the welds can be explained from the Al–Cu binary phase diagram with the assumption that complete phase equilibrium is reached in the liquid state but not during solidification. The primary dendrites α-Al, $CuAl_2$, CuAl, and a eutectic of α-Al/$CuAl_2$ are formed in the weld nugget during solidification. The nucleation and growth of Cu_9Al_4 is probably due to the mechanical mixing in the solid state, and the dissolution and interdiffusion of aluminum and copper at an elevated temperature.

Acknowledgements

This work was financially supported by the U.S. Department of Education, Grant No. P200A80806-98, by the Brown Foundation, Houston, TX and by SMU. The authors are also grateful for the technical support of Mr. Valant, Mr. Song, and Mrs. Jandric.

References

[1] L.E. Murr, R.D. Flores, O.V. Flores, J.C. McClure, G. Liu, D. Brown, Friction stir welding: microstructural characterization, Mater. Res. Innovation 1 (4) (1998) 211–223.
[2] W.B. Lee, S.B. Jung, Void free friction stir weld zone of the dissimilar 6061 aluminum and copper joint by shifting the tool insertion location, Mater. Res. Innovation 8 (2) (2003) 93–96.

[3] M. Aritoshi, K. Okita, T. Enjo, K. Ikeuchi, F. Matsuda, Friction welding of oxygen free copper to pure aluminum, Q. J. Jpn Welding Soc. 9 (4) (1991) 467–474.

[4] M. Aritoshi, K. Okita, T. Enjo, K. Ikeuchi, F. Matsuda, T. Tomita, Friction welding of copper–tungsten sintered alloy to pure titanium, Q. J. Jpn Welding Soc. 9 (4) (1991) 481–488.

[5] M. Abbasi, A. Karimi Taheri, M.T. Salehi, Growth rate of intermetallic compounds in Al/Cu bimetal produced by cold roll welding process, J. Alloys Compd. 319 (2001) 233–241.

[6] B.S. Yilbas, A.Z. Sahin, N. Kahraman, A.Z. Al-Garni, Friction welding of steel–Al and Al–Cu materials, J. Mater. Process. Technol. 49 (1995) 431–443.

[7] C.J. Dawes, Mirco-friction welding aluminum studs to mild steel plates, Metal Construction 9 (5) (1977) 196–197.

[8] O.T. Midling, Φ. Grong, A process model for friction welding of Al–Mg–Si alloys and Al–SiC metal matrix composites-I. HAZ temperature and strain rate distribution, Acta Metall. Mater. Trans. 42 (5) (1994) 1595–1609.

[9] L.E. Murr, Li Ying, E.A. Trillo, R.D. Flores, J.C. McClure, Microstructure in friction stir welded metals, J. Mater. Process. Manuf. Sci. 7 (1998) 145–161.

[10] Li. Ying, E.A. Trillo, L.E. Murr, Friction stir welding of aluminum alloy 2024 to silver, J. Mater. Sci. Lett. 19 (2000) 1047–1051.

[11] L.E. Murr, Li. Ying, E.A. Trillo, J.C. McClure, Fundamental issues and industrial applications of friction stir welding, Mater. Technol. 15 (1) (2000) 37–48.

[12] L.E. Murr, E.A. Trillo, Y. Li, R.D. Flores, B.M. Nowak, J.C. McClure, in: N. El-Kaddah, et al. (Eds.), Solid State Flow Associated with the Friction Stir Welding of Dissimilar Metals, in Fluid Flow Phenomena in Metals Processing, The Minerals Metals & Materials Society, 1999, pp. 31–40.

[13] W. Tang, X. Guo, J.C. McClure, L.E. Murr, Heat input and temperature distribution in friction stir welding, J. Mater. Process. Manufact. Sci. 7 (1998) 163–172.

[14] M.W. Mahoney, C.G. Rhodes, J.G. Flintoff, R.A. Spurling, W.H. Bingel, Properties of Friction Stir Welded 7075 T651 Aluminum, Metall. Trans. A 29A (1998) 1955–1964.

[15] A.P. Reynolds, W.D. Lockwood, T.U. Seidel, Processing-property correlation in friction stir welds, Mater. Sci. Forum 331–337 (2000) 1719–1724.

[16] M. Arvind, P. Yu, M.Y. Yau, H.L. Dickon, Ng, formation of Al_2Cu and AlCu intermetallics in Al9Cu alloy matrix composites by reaction sintering, Mater. Sci. Eng. A 380 (2004) 384–393.

[17] ASM Handbooks, vol. 3, Alloy Phase Diagrams, ASM International, Materials Park, Ohio, 2002.